MITOGEN-ACTIVATED PROTEIN KINASES ARE INVOLVED IN HEPATOCANALICULAR DYSFUNCTION AND CHOLESTASIS INDUCED BY OXIDATIVE STRESS

Flavia .D. Toledo[1], Cecilia L. Basiglio[1], Ismael R. Barosso[1], Andrea C. Boaglio[1], Andrés E. Zucchetti[1], Enrique J. Sánchez Pozzi[1], and Marcelo G. Roma[1]

[1]*Instituto de Fisiología Experimental (IFISE-CONICET), Facultad de Ciencias Bioquímicas y Farmacéuticas, University of Rosario, Rosario, Argentina*

Author for correspondence:

Dr. Marcelo G. Roma
Instituto de Fisiología Experimental (IFISE)
Facultad de Ciencias Bioquímicas y Farmacéuticas (UNR)
Suipacha 570, 2000 – Rosario, ARGENTINA
Tel.: +54-341-4305799
Fax: +54-341-4399473
E-mail: mroma@fbioyf.unr.edu.ar

ABSTRACT

In previous studies, we showed that the pro-oxidant model agent *tert*-butyl hydroperoxide (*t*BuOOH) induces alterations in hepatocanalicular secretory function by activating Ca^{2+}-dependent protein kinase C isoforms (cPKC), via F-actin disorganization followed by endocytic internalization of canalicular transporters relevant to bile formation (Mrp2, Bsep). Since mitogen-activated protein kinases (MAPKs) may be downstream effectors of cPKC, we investigated here the involvement the MAPKs of the ERK1/2, JNK1/2, and $p38^{MAPK}$ types in these deleterious effects. *t*BuOOH (100 µM, 15 min) increased the proportion of the active, phosphorylated forms of ERK1/2, JNK1/2, and $p38^{MAPK}$, and panspecific PKC inhibition with bisindolylmaleimide-1 (100 nM) or selective cPKC inhibition with Gö6976 (1 µM) prevented the latter two events. In isolated rat hepatocyte couplets, *t*BuOOH decreased the canalicular vacuolar accumulation of the fluorescent Bsep and Mrp2 substrates, cholylglycylamidofluorescein and glutathione-methylfluorescein, respectively, and selective inhibitors of ERK1/2 (PD098059), JNK1/2 (SP600125), and $p38^{MAPK}$ (SB203580) partially prevented these alterations. In *in situ* perfused rat livers, these three MAPK inhibitors prevented *t*BuOOH (75 µM)-induced impairment of bile flow, and the decrease in the biliary output of the Bsep and Mrp2 substrates, taurocholate and dinitrophenyl-*S*-glutathione, respectively. The changes in Bsep/Mrp2 and F-actin localization induced by *t*BuOOH, as assessed by (immuno)fluorescence staining followed by analysis of confocal images, were prevented total or partially by the MAPK inhibitors. We concluded that MAPKs of the ERK1/2, JNK1/2, and $p38^{MAPK}$ types are all involved in cholestasis induced by oxidative stress, by

promoting F-actin rearrangement and further endocytic internalization of canalicular transporters critical for bile formation.

KEYWORDS: Oxidative stress, hepatocellular cholestasis, canalicular transporters, mitogen-activated protein kinases, actin cytoskeleton.

INTRODUCTION

Oxidative stress (OS) is a common feature in most hepatopathies, including drug and environmental toxin-induced hepatotoxicity, hepatic ischemia-reperfusion injury, viral and autoimmune hepatitis, alcoholic and non-alcoholic steatohepatitis, and pathologies leading to hepatic accumulation of either heavy metals, such as iron (hemochromatosis) and copper (Wilson´s disease), or bile acids (obstructive or functional cholestasis) (Copple 2010; Jaeschke 2002).

In recent years, evidence has accumulated that, in cholestatic hepatopathies, a vicious circle occurs, since OS is cholestatic in nature, thus aggravating the initial secretory failure (Roma 2008). Indeed, our group demonstrated in isolated rat hepatocyte couplets (IRHCs) that OS induces rapid endocytic internalization of the bile salt export pump (Bsep, *AKA:* Abcc11) (Perez 2006b), the main canalicular bile salt transporter. A similar phenomenon was described for multidrug resistance-associated protein 2 (Mrp2, Abcc2) (Schmitt 2000; Sekine 2011; Ji 2004), another canalicular transporter highly relevant to bile formation by mediating the biliary excretion of glutathione, another main driving force of bile formation.

We also showed a close link between internalization of canalicular transporters and actin cytoskeleton disarrangement, an alteration that has been shown to onset canalicular transporter endocytosis (Rost 1999). Under OS conditions, actin redistributes from the pericanalicular zone to the rest of cell body, through a mechanism involving calcium-dependent isoenzymes of protein kinase C (cPKC) (Perez 2006a, b); this may occur via both an increase of intracellular calcium levels (Stone 1994) and a direct activation of cPKC via oxidative modifications (Cosentino-Gomes 2012).

The exact mechanisms that explain the deleterious effect of cPKC on actin integrity and, by extension, on the hepatocanalicular function have not been yet elucidated. PKC may activate downstream signaling pathways able to intermediate cytoskeletal perturbations, and the signaling pathways mediated by mitogen-activated protein kinases (MAPKs) are likely candidates; our previous finding that PKA activation counteracts OS-induced hepatocanalicular dysfunction (Perez 2006a, b) also points to MAPKs, since PKA exerts inhibitory cross-talk on MAPK activation (Cook 1993).

MAPKs are evolutionarily conserved serine/threonine-specific protein kinases involving three major subfamilies, namely extracellular signal-regulated kinases (ERK1/2, ERK3/4, ERK5, ERK7/8), Jun N-terminal kinases (JNK1/2/3), and $p38^{MAPK}$ ($p38^{MAPK}$ α/β/γ/δ) (Kyriakis 2012). They respond to a wide range of hormones and extracellular stressors, including OS (Kyriakis 2012). After recognition of these effectors by surface receptors, MAPKs are activated by three-tiered, sequential phosphorylations mediated by small GTP-binding proteins (*e.g.*, Ras, Rap) and two further protein kinases (MAPKKK and MAPKK), which act as dual-specificity enzymes that activate a selective MAPK type. Non-canonical activation of MAPKs also exists, via either MAPK autophosphorylation or direct MAPK phosphorylation by alternative protein kinases, such as Src or ZAP70 (Pimienta 2007).

Activation of MAPKs are triggered by OS in most organs, including liver (Kyriakis 2012). Radical oxygen species (ROS) from different sources induced ERK1/2, JNK1/2, and $p38^{MAPK}$ activation in murine hepatocytes (Rosseland 2005; Conde de la 2006; Abdelmegeed 2004), as well as in hepatoma cell lines (Nguyen 2013; Liu 2011). Similarly, PKC can activate MAPKs in hepatocytes (Romanelli 1997), an effect that is thought to be

mediated by Ras (Malumbres 1998). More relevant to our case, MAPKs are activated by PKC under OS conditions in hepatocytes (Lee 2008; Gao 2004).

This prompt us to hypothesize that MAPKs are involved in OS-induced, cPKC-mediated impairment of the hepatocalicular function and cholestasis. To confirm this contention, we analyzed the role for MAPKs in cholestasis induced by the pro-oxidizing compound *t*BuOOH, in two *in vitro* models for the study of biliary secretion, namely IRHCs and *in situ* perfused rat livers (PRLs). *t*BuOOH is a short chain analogue of lipid peroxides widely used to mimic the deleterious effect lipid peroxides produced during the OS-induced lipid oxidation cascade; like endogenous lipid peroxides, *t*BuOOH generate, after metabolic activation, peroxyl and alkoxyl radicals, with the former being most likely involved in cholestatic effects (Ahmed-Choudhury 1998).

MATERIALS AND METHODS

Materials.

Collagenase type A (from *Clostridium histolyticum*), bovine serum albumin (fraction V), *t*BuOOH, dimethyl sulfoxide (DMSO), 1-chloro-2,4-dinitrobenzene (CDNB), sodium taurocholate, trypan blue, Leibovitz-15 (L-15) culture medium, ethylene glycol tetraacetic acid, tetramethylethylenediamine, urethane, phenylmethylsulfonyl fluoride (PMSF), reduced nicotinamide adenine dinucleotide phosphate, and Triton X-100 were purchased from Sigma Chemical Co. (St. Louis, MO, USA). 5-Chloromethylfluorescein diacetate (CMFDA), Alexa Fluor 568 phalloidin were from Molecular Probes (Eugene, OR, EE.UU.). Gö6976, bisindolylmaleimide-1 (BIM-1), PD980589, SB203580, and SP600125 were from Calbiochem (San Diego, CA, EE.UU.). Dulbecco´s Modified Eagle Medium (DMEM) culture medium was from Life Technologies (Grand Island, NY, EE.UU.). Rabbit antimouse Bsep (1:100) antibody was from Kamiya (Seattle, Washington, USA). Primary anti-MRP2 antibody (M2 III-6 clone) was from Alexis Biochemicals (San Diego, CA, EE.UU.). Secondary, horseradish peroxidase (HRP)-conjugated anti-rabbit IgG and anti-mouse IgG antibodies, chemiluminescent substrate for HRP, and Hyperfilm ECL were from Thermo Fisher Scientific Inc. (Waltham, MA, EE.UU.). Secondary, Cy2-conjugated anti-rabbit and anti-mouse IgG antibodies were from Jackson InmunoResearch Laboratories, Inc (Filadelfia, EE.UU.). Mouse anti-$p38^{MAPK}$ and rabbit anti-phosphorylated $p38^{MAPK}$ were from Santa Cruz Biotechnology (Santa Cruz, CA, EE.UU.). Rabbit anti-phosphorylated ERK1/2, rabbit anti-ERK1/2, rabbit anti-JNK1/2, and mouse anti-phosphorylated JNK1/2 antibodies were from Cell Signaling Technology (Danvers, MA,

EE.UU.). Cholylglycyl amidofluorescein (CGamF) was kindly donated by Prof. Alan Hofmann (University of California, San Diego, CA, EE.UU.). All the other reagents were of the highest purity commercially available.

Animals.

Adult male Wistar rats weighing 300-350 g (8- to 10-weeks-old) were used throughout. Animals were maintained on a standard diet and water *ad libitum*, and housed in a temperature- and humidity-controlled room under a constant 12-hour light, 12-hour dark cycle. Treatments were carried out under urethane anesthesia (1 g/kg, i.p.). All animals received humane care according to the criteria outlined in the "Guide for the Care and Use of Laboratory Animals", by the National Academy of Sciences and published by the National Institutes of Health (NIH publication 25-28, revised 1996).

Western blot analysis of MAPK phosphorylation

Activation of $p38^{MAPK}$, ERK1/2, and JNK1/2 was assessed by evaluating by Western blotting the phosphorylation status of these MAPKs in lysates of primary-cultured rat hepatocytes. Briefly, isolated rat hepatocytes were obtained by collagenase perfusion, as described elsewhere (Berry 1969), and cultured in 3-cm Petri dishes with DMEM medium supplemented with 10% FCS and antibiotics (penicillin, streptomycin), at the density of 2 x 10^6 cells/mL. After 24 hs of culture, cells were exposed to *t*BuOOH (100 µM) for 5, 15, and 30 min, or for 15 min in cells pretreated for 15 min with the cPKC inhibitor Gö6976 (1 µM) (Perez 2006a, b) or the panspecific PKC inhibitor BIM-1 (100 nM) (Zegers 1997), washed with cold phosphate-buffered saline, and finally resuspended in cell lysis buffer and

protease inhibitor cocktail. Aliquots containing equivalent total protein content, as determined by the Lowry procedure with BSA as the standard (Lowry 1951), were subjected to sodium dodecyl sulfate/12% polyacrylamide gel electrophoresis, electrotransferred to Immobilon-P membranes and probed overnight with rabbit anti-phosphorylated $p38^{MAPK}$ (1:300), rabbit anti-phosphorylated ERK1/2 (1:1000), and mouse anti-phosphorylated JNK1/2 (1:2000) antibodies. Stripped membranes were reprobed with rabbit anti-total $p38^{MAPK}$ (1:1000), rabbit anti-total ERK1/2 (1:1000), and mouse anti-total JNK1/2 (1:1000) antibodies. After exposure to donkey anti-rabbit IgG secondary antibody or a goat anti-mouse IgG (1:5000, 1 h; Thermo Fisher Scientific, Waltham, MA, USA), protein bands were visualized using a chemiluminescence reagent (ECL™-GE Healthcare, USA) and captured with Hyperfilm ECL™ (GE Healthcare, Amersham, USA); the autoradiography film was manually scanned, and the densitometry data were obtained by using the ImageJ 1.34m software (NIH, USA).

Studies in isolated rat hepatocyte couplets

Couplets isolation, enrichment, culture, and treatments. IRHCs were obtained according to the two-step collagenase perfusion procedure, followed by centrifugal elutriation (Wilton 1991). The resulting preparation, containing 70 ± 4% of couplets of high viability (>95%), was plated onto 24-well plastic plates, at a density of 5×10^4 units/ml, and incubated at 37 ºC for 4.5 h, for attachment and repolarization. Then, IRHCs were incubated with *t*BuOOH (100 μM, 15 min), or DMSO (vehicle; 0.2-0.5 % v/v) in controls; at the 100 μM concentration, *t*BuOOH had been shown to impair by ~50% the Bsep-mediated canalicular transport function in IRHCs (Ahmed-Choudhury 1998), whereas 0.5 % v/v DMSO was

without effect on this parameter (Perez 2006a), and on blebbing/actin organization (Perez 2006b).

To assess the involvement of MAPK in the deleterious effect induced by *t*BuOOH, the MAPK inhibitors SB203580 (1 µM, $p38^{MAPK}$ inhibitor), PD098059 (50 µM, MEK inhibitor) or SP600125 (1 µM, JNK inhibitor) was added to the culture medium for 15 min prior to exposure to *t*BuOOH, and kept further during the exposure to this pro-oxidant compound.

Assessment of biliary secretory function in IRHCs. Bsep function was evaluated by assessing the proportion of couplets (> 200 per preparation) displaying canalicular vacuolar accumulation (CVa) of the fluorescent bile salt analog CGamF, a fluorescent Bsep substrate (Maglova 1995), as described previously (Basiglio 2014). Similarly, Mrp2 function was evaluated through its ability to secrete glutathione-*S*-methylfluorescein (GS-MF), the fluorescent glutathione-conjugated metabolite of CMFDA; this latter compound diffuses passively, and is intracellularly metabolized by esterases and glutathione *S*-transferases to render GS-MF (Roelofsen 1998).

Assessment of bleb formation. Blebbing, a preliminary marker of F-actin cytoskeleton disruption (Gores 1990), was quantified using light microscopy, by assessing the proportion of IRHCs exhibiting at least one bleb in either of the two cells, referred to the total number of IRHCs analyzed (> 50) (Stone 1994).

Bsep, Mrp2, and F-actin localization. Bsep and Mrp2 immunostaining was carried out as described elsewhere (Crocenzi 2008). Briefly, paraformaldehyde-fixed IRHCs were incubated with antibodies to Bsep or Mrp2 (1:100) for 2 h, followed by incubation with Cy2-labeled anti-rabbit (or anti-mouse) IgG goat antibody (1:200), or with Alexa Fluor 568

phalloidin for F-actin, for a further 40-min period. Densitometric analysis of confocal images taken with a Zeiss Pascal LSM 5 (Carl Zeiss, Walldorf, Germany) was carried out to assess the localization of both Bsep/Mrp2 and F-actin. The canalicular vacuole was delimited by superposing each fluorescence image with its respective differential interface contrast (DIC) image (Boaglio 2012). Intensity of Bsep/Mrp2-associated fluorescence was quantified along an 8-µm line perpendicular to the canalicular vacuole (from -4 µm to +4 µm of the canalicular center), as described elsewhere (Boaglio 2012). The proportion of F-actin confined in its normal pericanalicular localization was also quantified. For this purpose, this pericanalicular region was delimited by determining the area surrounding the bile canaliculi of control IRHCs where the pixels had a F-actin-associated fluorescence intensity at least twice of that of the background. This area was no wider than 1 µm, a value close to that reported elsewhere (Serriere 2008).

Studies in PRLs.

Rat liver perfusion. Livers from bile duct-cannulated rats (Intramedic PE-10 tubing, Clay Adams) were perfused *in situ* in a non-recirculating system, as described elsewhere (Crocenzi 2008). Experiments exhibiting lactate dehydrogenase activities > 20 U/L in the perfusate outflow were considered unviable.

After a 20-min stabilization period, SB203580 (250 nM), PD98059 (5 µM), SP600125 (1 µM), or their solvent, DMSO, was added, and allowed to act throughout the whole perfusion period. After 15 min of pretreatment with each MAPK inhibitor, *t*BuOOH (or DMSO) was added to the reservoir at a 75 µM concentration, and allowed to act for a further 10-min period. Finally, *t*BuOOH perfusion was stopped, and the livers were

perfused only with each of the MAPK inhibitors. Bile was collected at 10-min intervals throughout the experiment.

Bile flow was estimated gravimetrically. We also calculated the outputs of the Bsep substrate taurocholate (added to the reservoir at a 2.5 μM concentration) and of the Mrp2 substrate 2,4-dinitrophenyl-*S*-glutathione (DNP-SG), produced intracellularly by glutathione conjugation of CDNB (added to the reservoir at a 0.5 μM concentration). Taurocholate was assessed in bile by the 3α-hydroxysteroid dehydrogenase procedure (Talalay 1960). Biliary DNP-SG was determined by HPLC, as described elsewhere (Mottino 2001). At the end of the experiment, livers were removed, sections were rapidly frozen in dry-ice-chilled isopentane, and stored at -70ºC, until use.

Immunohistochemical detection of Bsep, Mrp2 and F-actin. Confocal microscopy was used to visualize Bsep/Mrp2 endocytic internalization and F-actin disorganization, as previously described (Basiglio 2014). Briefly, liver slices (5 μm) were prepared with a Zeiss Microm HM500 microtome cryostat, and fixed for 10 min with 3% paraformaldehyde, in PBS. For Bsep and Mrp2 labeling, tissue sections were incubated overnight with the specific antibody to Bsep or Mrp2 (1:100). Sections were then incubated with Cy2-conjugated donkey anti-rabbit IgG (1:100) and Alexa Fluor 568 phalloidin (for F-actin staining), for 1 h. Then, slices were mounted, and analyzed by confocal microscopy.

Statistical analysis.

Statistical analysis was performed by using GraphPad Prism software (GraphPad, San Diego, CA, USA). Results were expressed as mean ± S.E.M. When requirements for parametric analysis were met, a Student's unpaired *t* test was used for comparison between

two groups; comparisons between two groups that did not meet this criterion were carried out using the Mann-Whitney's rank sum test. Multiple groups were compared by one-way analysis of variance (ANOVA) or, when normality test failed, by non-parametric Kruskal-Wallis' test (one-way ANOVA by ranks). If ANOVA reached any statistical significance among groups, pairwise multiple comparisons were carried out by using Tukey's or Dunn's tests, respectively. The variances of the densitometric profiles of Bsep and Mrp2 localization were compared with the Mann-Whitney U test. *p* values lower than 0.05 were judged to be significant.

RESULTS

MAPK activation by tBuOOH, and dependency on cPKC.

The time course of $p38^{MAPK}$, ERK1/2 and JNK1/2 after exposure of cultured rat hepatocytes to *t*BuOOH, as determined by the increase in the phosphorylated, active forms of these enzymes, is shown in Fig. 1 *A*. Western blots of phospho- (p)-ERK1/2, p-JNK1/2, and, $p\text{-}p38^{MAPK}$ showed that *t*BuOOH increased the amount of the each p-MAPK in a time-dependent manner, with increments becoming apparent by 5 min after *t*BuOOH exposure.

As shown in Fig. 1 *B*, pretreatment with the cPKC inhibitor Gö6976 selectively prevented the increase in $p\text{-}p38^{MAPK}$ and p-JNK1/2, but no that of p-ERK1/2, indicating that activation of $p38^{MAPK}$ and JNK1/2 depends upon cPKC, whereas activation of ERK1/2 depends on an alternative, unidentified redox-sensitive signaling pathway. To control for putative Gö6976 inhibitory unspecificity towards other redox-sensitive kinases, the structurally and mechanistically unrelated PKC inhibitor bisindolylmaleimide-1 (BIM-1) was assayed as well, and they inhibited $p38^{MAPK}$ and JNK1/2 to the same extent as Gö6976.

MAPKs play a role in tBuOOH-induced impairment of function and localization of Bsep and Mrp2 in IRHCs.

The percentage of couplets able to accumulate in their canalicular vacuoles the fluorescent Bsep and Mrp2 substrates CGamF and GS-MF, respectively, is shown in Fig. 2. Control couplets exposed only to DMSO (*t*BuOOH vehicle) showed a 65-70% CVa of each fluorescent substrate. While *t*BuOOH caused a decrease in the percentage of couplets accumulating apically both fluorescent substrates, pre-treatment with the JNK1/2 inhibitor

SP600125 (1 μM), the ERK inhibitor PD098059 (5 μM and 50 μM), and the $p38^{MAPK}$ inhibitor SB203580 (1 μM) partially prevented these effects. None of these inhibitors modified the apical accumulation of both substrates *per se* (Supplementary Table 1).

Confocal immunolocalization studies in control IRHCs showed that both Bsep and Mrp2 were mainly confined to the canalicular membrane, while *t*BuOOH induced relocalization of Bsep and Mrp2 into intracellular vesicles, indicating endocytosis (Fig. 3, upper graphs of panels *A* and *B*, respectively). All the MAPKs inhibitors partially prevented this effect.

These findings were confirmed by densitometric analysis. Densitometric curves showed a flatter Bsep and Mrp2 fluorescence profile in *t*BuOOH-treated IRHCs, as compared to controls (Fig. 3, lower graphs of panels *A* and *B*, respectively). In IRHCs pretreated with either of the MAPK inhibitors, densitometric curves were statistically less flat than that of *t*BuOOH alone ($p<0.05$).

MAPKs are involved in tBuOOH-induced blebbing and F-actin redistribution.

Bleb formation was assessed as a preliminary marker of cytoskeleton disruption (Gores 1990), by phase-contrast microscopy. As shown in Fig. 4 *A*, control cells exposed only to the *t*BuOOH solvent, DMSO, showed a low background blebbing (< 18%), which consisted usually of a single, small bleb per cell (type 1 blebbing). In contrast, *t*BuOOH induced extensive bleb formation, often visualized as multiple membrane protrusions distributed all over the cell surface (type 2 blebbing). Individual pretreatment with all the MAPK inhibitors fully prevented this effect. None of these inhibitors induced blebbing *per se* (Supplementary Table 1)

F-actin distribution was also analyzed by confocal microscopy under the same conditions (Fig. 4 *B*). In control IRHCs, F-actin displayed a predominant pericanalicular localization, forming a dense belt beneath the canalicular membrane. In *t*BuOOH-treated IRHCs, bleb formation was accompanied by extensive redistribution of F-actin from the pericanalicular area to the sinusoidal plasma membrane region. Redistribution of F-actin was extensively prevented by pretreatment of IRHCs with either of the MAPK inhibitors.

tBuOOH induces cholestasis by a MAPK-mediated mechanism in PRLs.

Livers were perfused first with *t*BuOOH (75 µM) for 10 min, in the presence or absence of the JNK1/2 inhibitor SP600125, the ERK inhibitor PD098059, and the $p38^{MAPK}$ inhibitor SB203580 (Fig. 5); 75 µM *t*BuOOH closely reproduced the extent of bile salt secretory failure reached in IRHCs exposed to 100 µM *t*BuOOH.

Initial exposure of PRLs to the MAPK inhibitors did not significantly influenced bile flow. On the other hand, bile flow dropped sharply after the onset of *t*BuOOH perfusion, with a nadir to ~60% of control values at 20 min, and a trend towards recovery of bile flow afterwards; this is likely due to both the efficient reductive detoxification of *t*BuOOH (Rush 1986) and the further spontaneous recovery of actin organization and canalicular transport function, which was shown to occur quickly in the IRHC model (Pérez 2006a, b). All the MAPK inhibitors significantly prevented this bile flow decrease, with bile flow profiles approaching that of control (Fig. 5 *A*).

Since Bsep and Mrp2 are key determinants of bile flow, we assessed the capability of the MAPK inhibitors to prevent their functional impairment induced by *t*BuOOH. The pro-oxidant induced a ~85% and a ~60% of decrease in the excretion of the Bsep and Mrp2

substrates taurocholate and DNP-SG, respectively, but this effect was prevented when the MAPK inhibitors were present (Fig. 5 *B* and *C*, respectively).

MAPKs are involved in the changes of Bsep, Mrp2, and F-actin localization induced by tBuOOH.

Tissue sections obtained from PRLs after 20 min of the onset of *t*BuOOH exposure were subjected to co-staining of Bsep and F-actin, or Mrp2 and F-actin. In control livers, transporter-associated fluorescence was confined to the canalicular space (Fig. 6). In *t*BuOOH-treated livers, the carriers relocalized from the canalicular space to the pericanalicular, as indicated by the increased fluorescence at a greater distance from the bile canaliculus. Exposure to ERK1/2, JNK1/2 and $p38^{MAPK}$ inhibitors significantly prevented these alterations.

DISCUSSION

In previous works, we demonstrated that *t*BuOOH induces alterations in the secretory function in IRHCs via activation of cPKC, through a mechanism that involve disorganization of the F-actin cytoskeleton, and subsequent endocytic internalization of canalicular transporters responsible for bile formation, Bsep and Mrp2 (Perez 2006a, b). In this work, we extended this finding by showing that MAPKs of the ERK1/2, JNK1/2, and $p38^{MAPK}$ types are all involved in OS-induced cholestasis as well, and that, for JNK1/2 and $p38^{MAPK}$, cPKC is an upstream activator. On the other hand, ERK1/2 activation by *t*BuOOH does not seem to be mediated by cPKC; this is in line with the finding that ERK1/2 was activated by hydrogen peroxide via Ca^{2+}- and PKC-independent mechanisms in cardiomyocytes, involving instead the Src family of tyrosine kinases Ras and Raf-1 (Aikawa 1997). Another possible redox sensitive kinase that can be involved upstream of ERK1/2 is *apoptosis stimulating kinase 1 (*ASK-1), a serine/threonine kinase of the MKKK family; ASK1 can be activated by ROS-mediated oxidation of its physiological inhibitor, thioredoxin, with whom ASK1 forms an inactive complex (Saitoh 1998).

Whether these MAPKs directly phosphorylates cytoskeletal proteins to induce F-actin relocalization and further impairment in canalicular transporter localization is unknown. There is accumulating evidence in other epithelial cell types that this may be the case. For example, ethanol induced disruption of F-actin and the subsequent opening of intercellular tight junctions through oxidative mechanisms in Caco-2 cells, a polarized *in vitro* model of intestinal epithelium (Elamin 2014) and, as in our case, the MAPKs of the $p38^{MAPK}$, ERK1/2, and JNK1/2 types need to be all active for this deleterious effect to occur. The event also involved the phosphorylation of myosin light chain kinase (MLCK),

which favors the formation of crosslinks with F-actin by phosphorylating myosin light chain (MLC); once phosphorylated, MLC generates a myosin-F-actin contractile force, with the resulting increase in cytoplasm tension and bleb formation (Elamin 2014). It has also been shown in livers subjected to ischemia/reperfusion that $p38^{MAPK}$ induces activation of heat shock protein 27 (HSP27) (Keller 2005), a protein that promotes the formation of crosslinks between F-actin and myosin by inhibiting the phosphorylation of caldesmon, a physiological inhibitor of the myosin-F-actin interaction (Somara 2006). In addition, ERK1/2 may directly phosphorylate caldesmon *in vivo*, thus reinforcing this effect (Hedges 2000). A similar phenomenon was reported in the human liver cell line HL7702 exposed to the phosphatase 2A inhibitor microcystin-LR, a toxin that promotes cytoskeletal reorganization by inducing $p38^{MAPK}$- and JNK1/2-mediated phophorylation of HSP27 (Sun 2011). In a pro-apoptotic context, MLC phosphorylation and the resulting bleb formation may also be mediated by the serine/threonine protein kinase ROCK I, which is activated by caspase-3-dependent cleavage (Sebbagh 2001). Although apoptosis is a well recognized event in hepatocytes exposed to high *t*BuOOH concentrations (Toledo 2014; Salkar 2010; Tripathi 2009), at the low concentration used here (100 µM), *t*BuOOH showed no sign of caspase-3 activation, as well as of other hallmarks of apoptosis, such as appearance of nuclei with subdiploid DNA content and cytochrome-*c* release (Gómez-Lechón 2002). However, bleb formation may precede these apoptotic changes (Barros 2003), and therefore we cannot rule that the blebbing and consequent canalicular dysfunction occurring at low *t*BuOOH levels may represent a very early event of an ongoing apoptotic process. Interestingly, Deschesnes et al. (2001) showed that blebbing in c-Myc–dependent apoptosis of rat-1 cells was independent of caspase activity, but depended on $p38^{MAPK}$-sensitive

changes in microfilament dynamics, likely mediated by HSP27 phosphorylation. The functional status of canalicular transporters during the apoptotic process and its relationship with the cytoskeletal perturbations induced by OS is a pending, intriguing issue that deserves further investigation.

MAPKs could also change canalicular transporter location by activating mechanisms leading to radixin phosphorylation. Expression of constructs that mimic a permanently phosphorylated (active) form of radixin in the polarized, hybrid hepatoblastoma/human fibroblast cell line WIF-B led to redistribution of radixin from the canalicular to the basolateral membrane, probably as a consequence of a more promiscuous interaction of its active, phosphorylated form with both apical and basolateral pools of F-actin; this would lead to relocation of the canalicular transporters (Suda 2011). Furthermore, activation of radixin by $p38^{MAPK}$-dependent phosphorylation of Thr-564 has been shown in several cell lines, through a signaling mechanism which, like in our case, involves PKC activation (Zhang 2014; Bogatcheva 2011). Contrarily to this view, an impaired rather than an enhanced phosphorylation of radixin has been proposed to account for Mrp2 endocytosis under OS conditions in IRHCs; this would involve protein phosphatase PP-1-dependent dephosphorylation of radixin via PKC-induced PP-1 activation, leading to instability of Mrp2 in the plasma membrane by loss of cross-linking with actin filaments (Sekine 2011). This latter view is somewhat difficult to reconcile with our finding of significant ERK1/2 activation, since PP-1 was shown to prevent this activation presumably by dephosphorylation of the upstream enzymes, MEK and Raf (Schaeffer 1999).

MAPK dependence of *t*BuOOH-induced cholestasis is somewhat paradoxical with previous works showing that ERK1/2 and $p38^{MAPK}$ are both involved in choleretic phenomena, such as those induced by tauroursodeoxycholate (TUDC) (Kurz 2001; Schliess 1997; Kubitz 2004) and cAMP (Schonhoff 2010). For example, TUDC stimulates excretion of the choleretic bile salt taurocholate via an integrin-dependent signaling pathway involving both Ras/Raf/MEK/ERK1/2 and Src/$p38^{MAPK}$ (Häussinger 2003), as a result of stimulation of the Bsep trafficking from Golgi to the canalicular membrane (Kubitz 2004). The reason for the paradoxical mediation of MAPKs of opposite (choleretic and cholestatic) effects on bile flow under normal and oxidative conditions, respectively, is unclear at present, but could be linked to the following reasons:

1) MAPKs activation is highly compartmentalized, requiring localization at specific sites of scaffold proteins to allow regional recruitment of the multiple components of the MAPK cascade (Canal 2011). In quiescent hepatocytes, Raf-1 and MEK are located only in early endosomes, which are the first endosomal compartment to receive endocytosed transporters (Pol 1998). Therefore, the rapid cholestatic effects induced by *t*BuOOH in our acute exposure model may involve events limited to "early" compartment, such as endocytosis of transporters to subapical endosomes. Contrarily, the choleretic effects involving trafficking of transporters from Golgi/post-Golgi compartments to the canalicular membrane would be a later event, occurring when trafficking of scaffold proteins to deeper levels is stimulated by the choleretic stimulus (Philips 2004).

2) The different array of activated/inhibited signaling cascades occurring in an oxidative context may result, when operating in concert with MAPKs, in opposite effects on bile secretion, as compared to those occurring in the normal cellular context where choleresis

occurs. A similar paradoxical phenomenon was shown by us for the cholestatic agent estradiol 17ß-glucuronide, which also required cPKC-dependent MAPK activation to induce cholestasis (Boaglio 2012).

3) Choleretic and cholestatic compounds (in this case, *t*BuOOH) might activate MAPK isoforms with opposite effects on bile flow. For example, α- and β-p38^{MAPK} isoforms mediate choleretic and cholestatic effects of bile salts, respectively (Anwer 2012; Schonhoff 2010).

4) As shown here, the three MAPK types need to be activated simultaneously by *t*BuOOH to exert its cholestatic effects, and this may not be the case for choleretic compounds; for example, the choleretic bile salt TUDC activates p38^{MAPK} and ERK1/2, but not JNK1/2 (Kurz 2001).

Although more studies are needed to determine with certainty the molecular mechanisms by which the MAPKs induced cholestasis when activated in an oxidative context, our results show that the interaction of MAPKs with actin cytoskeleton is critical for the endocytic internalization of canalicular carriers relevant for bile formation, thus explaining the cholestatic phenomenon. Drugs that selectively inhibit MAPKs are used in preclinical and clinical studies with reasonable success (Chapman 2011). Given the existence of clinical cholestatic liver diseases in humans associated with high levels of OS, our results may help to envisage complementary therapeutic strategies to treat these diseases by using therapeutic tools that are already within our reach.

ACKNOWLEDGEMENTS

This work was supported by grants from Agencia Nacional de Promoción Científica y Tecnológica (ANPCyT) and Consejo Nacional de Investigaciones Científicas y Técnicas (CONICET) to Dr. Marcelo G. Roma. We thank Drs. Marcelo Luquita, Diego Taborda, and Rodrigo Vena for their valuable technical assistance in HPLC determinations, surgical procedures and confocal imaging, respectively.

REFERENCES

Abdelmegeed MA, Kim SK, Woodcroft KJ, Novak RF (2004) Acetoacetate activation of extracellular signal-regulated kinase 1/2 and p38 mitogen-activated protein kinase in primary cultured rat hepatocytes: role of oxidative stress. J Pharmacol Exp Ther 310:728-736. doi:10.1124/jpet.104.066522

Ahmed-Choudhury J, Orsler DJ, Coleman R (1998) Hepatobiliary effects of tertiary-butylhydroperoxide (tBOOH) in isolated rat hepatocyte couplets. Toxicol Appl Pharmacol 152:270-275. doi:10.1006/taap.1998.8495

Aikawa R, Komuro I, Yamazaki T, Zou Y, Kudoh S, Tanaka M, Shiojima I, Hiroi Y, Yazaki Y (1997) Oxidative stress activates extracellular signal-regulated kinases through Src and Ras in cultured cardiac myocytes of neonatal rats. J Clin Invest 100:1813-1821. doi:10.1172/JCI119709

Anwer MS (2012) Intracellular signaling by bile acids. J Biosci (Rajshari) 20:1-23. doi:10.3329/jbs.v20i0.17647

Barros LF, Kanaseki T, Sabirov R, Morishima S, Castro J, Bittner CX, Maeno E, Ando-Akatsuka Y, Okada Y. Apoptotic and necrotic blebs in epithelial cells display similar neck diameters but different kinase dependency. Cell Death Differ 10:687-697, 2003. doi:10.1038/sj.cdd.4401236

Basiglio CL, Toledo FD, Boaglio AC, Arriaga SM, Ochoa JE, Sanchez Pozzi EJ, Mottino AD, Roma MG (2014) Physiological concentrations of unconjugated bilirubin prevent oxidative stress-induced hepatocanalicular dysfunction and cholestasis. Arch Toxicol 88:501-514. doi:0.1007/s00204-013-1143-0

Berry MN, Friend DS (1969) High-yield preparation of isolated rat liver parenchymal cells: a biochemical and fine structural study. J Cell Biol 43: 506-520. doi:10.1083/jcb.43.3.506

Boaglio AC, Zucchetti AE, Toledo FD, Barosso IR, Sanchez Pozzi EJ, Crocenzi FA, Roma MG (2012) ERK1/2 and p38 MAPKs are complementarily involved in estradiol 17ß-D-glucuronide-induced cholestasis: crosstalk with cPKC and PI3K. PLoS One 7:e49255. doi:10.1371/journal.pone.0049255

Bogatcheva NV, Zemskova MA, Gorshkov BA, Kim KM, Daglis GA, Poirier C, Verin AD (2011) Ezrin, radixin, and moesin are phosphorylated in response to 2-methoxyestradiol and modulate endothelial hyperpermeability. Am J Respir Cell Mol Biol 45:1185-1194. doi:10.1165/rcmb.2011-0092OC

Canal F, Palygin O, Pankratov Y, Correa SA, Muller J (2011) Compartmentalization of the MAPK scaffold protein KSR1 modulates synaptic plasticity in hippocampal neurons. FASEB J 25:2362-2372. doi:10.1096/fj.10-173153

Chapman MS, Miner JN (2011) Novel mitogen-activated protein kinase kinase inhibitors. Expert Opin Investig Drugs 20:209-220. doi:10.1517/13543784.2011.548803

Conde de la RL, Schoemaker MH, Vrenken TE, Buist-Homan M, Havinga R, Jansen PL, Moshage H (2006) Superoxide anions and hydrogen peroxide induce hepatocyte death by different mechanisms: involvement of JNK and ERK MAP kinases. J Hepatol 44:918-929. doi:10.1016/j.jhep.2005.07.034

Cook SJ, McCormick F (1993) Inhibition by cAMP of Ras-dependent activation of Raf. Science 262:1069-1072. doi:10.1126/science.7694367

Copple BL, Jaeschke H, Klaassen CD (2010) Oxidative stress and the pathogenesis of cholestasis. Semin Liver Dis 30:195-204. doi:10.1055/s-0030-1253228

Cosentino-Gomes D, Rocco-Machado N, Meyer-Fernandes JR (2012) Cell signaling through protein kinase C oxidation and activation. Int J Mol Sci 13:10697-10721. doi:10.3390/ijms130910697

Crocenzi FA, Sanchez Pozzi EJ, Ruiz ML, Zucchetti AE, Roma MG, Mottino AD, Vore M (2008) Ca^{2+}-dependent protein kinase C isoforms are critical to estradiol 17ß-D-glucuronide-induced cholestasis in the rat. Hepatology 48:1885-1895. doi:10.1002/hep.22532

Elamin E, Masclee A, Troost F, Pieters HJ, Keszthelyi D, Aleksa K, Dekker J, Jonkers D (2014) Ethanol impairs intestinal barrier function in humans through mitogen activated protein kinase signaling: a combined in vivo and in vitro approach. PLoS One 9:e107421. doi:10.1371/journal.pone.0107421

Gao Y, Shan YQ, Pan MX, Wang Y, Tang LJ, Li H, Zhang Z (2004) Protein kinase C-dependent activation of P44/42 mitogen-activated protein kinase and heat shock protein 70 in signal transduction during hepatocyte ischemic preconditioning. World J Gastroenterol 10:1019-1027. doi:10.3748/wjg.v10.i7.1019

Gómez-Lechón MJ, O'Connor E, Castell JV, Jover R (2002) Sensitive markers used to identify compounds that trigger apoptosis in cultured hepatocytes. Toxicol Sci 65: 299-308. doi:10.1093/toxsci/65.2.299.

Gores GJ, Herman B, Lemasters JJ (1990) Plasma membrane bleb formation and rupture: a common feature of hepatocellular injury. Hepatology 11:690-698.

Häussinger D, Kurz AK, Wettstein M, Graf D, vom DS, Schliess F (2003) Involvement of integrins and Src in tauroursodeoxycholate-induced and swelling-induced choleresis. Gastroenterology 124:1476-1487. doi:10.1016/S0016-5085(03)00274-9

Hedges JC, Oxhorn BC, Carty M, Adam LP, Yamboliev IA, Gerthoffer WT (2000) Phosphorylation of caldesmon by ERK MAP kinases in smooth muscle. Am J Physiol Cell Physiol 278:C718-C726.

Jaeschke H, Gores GJ, Cederbaum AI, Hinson JA, Pessayre D, Lemasters JJ (2002) Mechanisms of hepatotoxicity. Toxicol Sci 65:166-176. doi:10.1093/toxsci/65.2.166

Ji B, Ito K, Sekine S, Tajima A, Horie T (2004) Ethacrynic-acid-induced glutathione depletion and oxidative stress in normal and Mrp2-deficient rat liver. Free Radic Biol Med 37:1718-1729. doi:10.1016/j.freeradbiomed.2004.08.020

Keller M, Gerbes AL, Kulhanek-Heinze S, Gerwig T, Grutzner U, van RN, Vollmar AM, Kiemer AK (2005) Hepatocyte cytoskeleton during ischemia and reperfusion--influence of ANP-mediated p38 MAPK activation. World J Gastroenterol 11:7418-7429. doi:10.3748/wjg.v11.i47.7418

Kubitz R, Sutfels G, Kuhlkamp T, Kolling R, Häussinger D (2004) Trafficking of the bile salt export pump from the Golgi to the canalicular membrane is regulated by the p38 MAP kinase. Gastroenterology 126:541-553. doi:10.1053/j.gastro.2003.11.003

Kurz AK, Graf D, Schmitt M, Vom Dahl S, Häussinger D (2001) Tauroursodeoxycholate-induced choleresis involves $p38^{MAPK}$ activation and translocation of the bile salt export pump in rats. Gastroenterology 121:407-419. doi:10.1053/gast.2001.26262

Kyriakis JM, Avruch J (2012) Mammalian MAPK signal transduction pathways activated by stress and inflammation: a 10-year update. Physiol Rev 92:689-737. doi:10.1152/physrev.00028.2011

Lee SH, Lee MY, Lee JH, Han HJ (2008) A potential mechanism for short time exposure to hypoxia-induced DNA synthesis in primary cultured chicken hepatocytes: Correlation between Ca^{2+}/PKC/MAPKs and PI3K/Akt/mTOR. J Cell Biochem 104:1598-1611. doi:10.1002/jcb.21657

Liu H, Xiao Y, Xiong C, Wei A, Ruan J (2011) Apoptosis induced by a new flavonoid in human hepatoma HepG2 cells involves reactive oxygen species-mediated mitochondrial dysfunction and MAPK activation. Eur J Pharmacol 654:209-216. doi:10.1016/j.ejphar.2010.12.036

Lowry OH, Rosembrough NJ, Farr AL, Randall RJ (1951) Protein measurement with the Folin phenol reagent. J Biol Chem 193: 265-275.

Maglova LM, Jackson AM, Meng XJ, Carruth MW, Schteingart CD, Ton-Nu HT, Hofmann AF, Weinman SA (1995) Transport characteristics of three fluorescent conjugated bile acid analogs in isolated rat hepatocytes and couplets. Hepatology 22:637-647. doi:10.1002/hep.1840220238

Malumbres M, Pellicer A (1998) RAS pathways to cell cycle control and cell transformation. Front Biosci 3:d887-d912.

Mottino AD, Hoffman T, Jennes L, Cao J, Vore M (2001) Expression of multidrug resistance-associated protein 2 in small intestine from pregnant and postpartum rats. Am J Physiol Gastrointest Liver Physiol 280:G1261-G1273.

Nguyen KC, Willmore WG, Tayabali AF (2013) Cadmium telluride quantum dots cause oxidative stress leading to extrinsic and intrinsic apoptosis in hepatocellular carcinoma HepG2 cells. Toxicology 306:114-123. doi:10.1016/j.tox.2013.02.010

Perez LM, Milkiewicz P, Ahmed-Choudhury J, Elias E, Ochoa JE, Sanchez Pozzi EJ, Coleman R, Roma MG (2006a) Oxidative stress induces actin-cytoskeletal and tight-junctional alterations in hepatocytes by a Ca2+ -dependent, PKC-mediated mechanism: protective effect of PKA. Free Radic Biol Med 40:2005-2017. doi:10.1016/j.freeradbiomed.2006.01.034

Perez LM, Milkiewicz P, Elias E, Coleman R, Sanchez Pozzi EJ, Roma MG (2006b) Oxidative stress induces internalization of the bile salt export pump, Bsep, and bile salt secretory failure in isolated rat hepatocyte couplets: a role for protein kinase C and prevention by protein kinase A. Toxicol Sci 91:150-158. doi:10.1093/toxsci/kfj113

Philips MR (2004) Sef: a MEK/ERK catcher on the Golgi. Mol Cell 15:168-169. doi:10.1016/j.molcel.2004.07.003

Pimienta G, Pascual J (2007) Canonical and alternative MAPK signaling. Cell Cycle 6:2628-2632. doi:10.4161/cc.6.21.4930

Pol A, Calvo M, Enrich C (1998) Isolated endosomes from quiescent rat liver contain the signal transduction machinery. Differential distribution of activated Raf-1 and Mek in the endocytic compartment. FEBS Lett 441:34-38. doi:10.1016/S0014-5793(98)01517-8

Roelofsen H, Soroka CJ, Keppler D, Boyer JL (1998) Cyclic AMP stimulates sorting of the canalicular organic anion transporter (Mrp2/cMoat) to the apical domain in hepatocyte couplets. J Cell Sci 111:1137-1145.

Roma MG, Sanchez Pozzi EJ (2008) Oxidative stress: a radical way to stop making bile. Ann Hepatol 7:16-33.

Romanelli A, van de Werve G (1997) Activation of mitogen-activated protein kinase in freshly isolated rat hepatocytes by both a calcium- and a protein kinase C-dependent pathway. Metabolism 46:548-555. doi:10.1016/S0026-0495(97)90193-1

Rosseland CM, Wierod L, Oksvold MP, Werner H, Ostvold AC, Thoresen GH, Paulsen RE, Huitfeldt HS, Skarpen E (2005) Cytoplasmic retention of peroxide-activated ERK provides survival in primary cultures of rat hepatocytes. Hepatology 42:200-207. doi:10.1002/hep.20762

Rost D, Kartenbeck J, Keppler D (1999) Changes in the localization of the rat canalicular conjugate export pump Mrp2 in phalloidin-induced cholestasis. Hepatology 29:814-821. doi:10.1002/hep.510290319

Rush GF, Alberts D (1986) *tert.*-Butyl hydroperoxide metabolism and stimulation of the pentose phosphate pathway in isolated rat hepatocytes. Toxicol Appl Pharmacol 85:324-331. doi:10.1016/0041-008X(86)90339-X

Saitoh M, Nishitoh H, Fujii M, Takeda K, Tobiume K, Sawada Y, Kawabata M, Miyazono K, Ichijo H (1998) Mammalian thioredoxin is a direct inhibitor of apoptosis signal-regulating kinase (ASK) 1. EMBO J 17:2596-2606. doi:10.1093/emboj/17.9.2596

Sarkar MK, Sil PC (2010) Prevention of tertiary butyl hydroperoxide induced oxidative impairment and cell death by a novel antioxidant protein molecule isolated from the herb, Phyllanthus niruri. Toxicol In Vitro 24:1711-1719. doi:10.1016/j.tiv.2010.05.014

Schaeffer HJ, Weber MJ (1999) Mitogen-activated protein kinases: specific messages from ubiquitous messengers. Mol Cell Biol 19:2435-2444. doi:10.1128/MCB.19.4.2435

Schliess F, Kurz AK, vom DS, Häussinger D (1997) Mitogen-activated protein kinases mediate the stimulation of bile acid secretion by tauroursodeoxycholate in rat liver. Gastroenterology 113:1306-1314. doi:10.1053/gast.1997.v113.pm9322526

Schmitt M, Kubitz R, Wettstein M, vom Dahl S, Häussinger D (2000) Retrieval of the mrp2 gene encoded conjugate export pump from the canalicular membrane contributes to cholestasis induced by tert-butyl hydroperoxide and chloro-dinitrobenzene. Biol Chem 381:487-495. doi:10.1515/BC.2000.063

Schonhoff CM, Webster CR, Anwer MS (2010) Cyclic AMP stimulates Mrp2 translocation by activating p38α MAPK in hepatic cells. Am J Physiol Gastrointest Liver Physiol 298:G667-G674. doi:10.1152/ajpgi.00506.2009

Sebbagh M, Renvoizé C, Hamelin J, Riché N, Bertoglio J, Bréard J (2001) Caspase-3-mediated cleavage of ROCK I induces MLC phosphorylation and apoptotic membrane blebbing. Nat Cell Biol. 3:346-352. doi:10.1038/35070019

Sekine S, Ito K, Saeki J, Horie T (2011) Interaction of Mrp2 with radixin causes reversible canalicular Mrp2 localization induced by intracellular redox status. Biochim Biophys Acta 1812:1427-1434. doi:10.1016/j.bbadis.2011.07.015

Serriere V, Tran D, Stelly N, Claret M, Alonso G, Tordjmann T, Guillon G (2008) Vasopressin-induced morphological changes in polarized rat hepatocyte multiplets: dual calcium-dependent effects. Cell Calcium 43:95-104. doi:10.1016/j.bbadis.2011.07.015

Somara S, Bitar KN (2006) Phosphorylated HSP27 modulates the association of phosphorylated caldesmon with tropomyosin in colonic smooth muscle. Am J Physiol Gastrointest Liver Physiol 291:G630-G639. doi:10.1152/ajpgi.00350.2005

Stone V, Johnson GD, Wilton JC, Coleman R, Chipman JK (1994) Effect of oxidative stress and disruption of Ca^{2+} homeostasis on hepatocyte canalicular function in vitro. Biochem Pharmacol 47:625-632. doi:10.1016/0006-2952(94)90124-4

Suda J, Zhu L, Karvar S (2011) Phosphorylation of radixin regulates cell polarity and Mrp-2 distribution in hepatocytes. Am J Physiol Cell Physiol 300:C416-C424. doi:10.1152/ajpcell.00467.2010

Sun Y, Meng GM, Guo ZL, Xu LH (2011) Regulation of heat shock protein 27 phosphorylation during microcystin-LR-induced cytoskeletal reorganization in a human liver cell line. Toxicol Lett 207:270-277. doi:10.1016/j.toxlet.2011.09.025

Talalay P (1960) Enzymatic analysis of steroid hormones. Methods Biochem Anal 8:119-143.

Toledo FD, Pérez LM, Basiglio CL, Ochoa JE, Sanchez Pozzi EJ, Roma MG (2014) The Ca^{2+}-calmodulin-Ca^{2+}/calmodulin-dependent protein kinase II signaling pathway is involved in oxidative stress-induced mitochondrial permeability transition and apoptosis in isolated rat hepatocytes. Arch Toxicol 88:1695-1709. doi:10.1007/s00204-014-1219-5.

Tripathi M, Singh BK, Kakkar P (2009) Glycyrrhizic acid modulates t-BHP induced apoptosis in primary rat hepatocytes. Food Chem Toxicol 47:339-347. doi:10.1016/j.fct.2008.11.028. Epub 2008 Nov 30.

Wilton JC, Williams DE, Strain AJ, Parslow RA, Chipman JK, Coleman R (1991) Purification of hepatocyte couplets by centrifugal elutriation. Hepatology 14:180-183. doi:10.1002/hep.1840140129

Zegers MM, Hoekstra D (1997) Sphingolipid transport to the apical plasma membrane domain in human hepatoma cells is controlled by PKC and PKA activity: a correlation with cell polarity in HepG2 cells. J Cell Biol 138:307-321. doi: 10.1083/jcb.138.2.307

Zhang C, Wu Y, Xuan Z, Zhang S, Wang X, Hao Y, Wu J, Zhang S (2014) p38MAPK, Rho/ROCK and PKC pathways are involved in influenza-induced cytoskeletal rearrangement and hyperpermeability in PMVEC via phosphorylating ERM. Virus Res 192:6-15. doi:10.1016/j.virusres.2014.07.027

FIGURE LEGENDS

FIGURE 1. ***Activation of MAPKs by tBuOOH, and its dependency on cPKC.*** (*A*) Time dependency of activation by *t*BuOOH (*t*Bu) of the MAPKs, ERK1/2 (left panel), JNK1/2 (central panel), and $p38^{MAPK}$ (right panel) in primary cultured hepatocytes exposed to *t*BuOOH (100 µM), or its vehicle (DMSO), for different time periods. MAPK activation was inferred from an increase in the phosphorylation status of these kinases, as assessed by Western blotting of the phospho-(p-)MAPK forms, using total (t)-MAPK forms as loading control (upper panel); phosphorylation degree was calculated as the p-MAPK-to-t-MAPK ratio for each experimental condition (lower panel), referred to control values. (*B*) Representative western blottings (upper panel) and densitometric analysis showing the dependency on cPKC activity of the activation of MAPKs by *t*BuOOH, as assessed by exposing primary cultured hepatocytes to the PKC inhibitors Gö6976 (Gö, 1 µM) or BIM-1 (100 nM) for 15 min, and then exposed to *t*BuOOH (100 µM) for a further 15-min period. Control group received only Gö/BIM-1 and *t*BuOOH vehicle (DMSO). The results are mean ± S.E.M., from 4 independent experiments. [a]Significantly different from control ($p < 0.05$); [b]Significantly different *t*BuOOH-treated hepatocytes ($p < 0.05$).

FIGURE 2. ***Protective effect of MAPK inhibitors on the altered Bsep and Mrp2 function induced by tBuOOH in IRHCs.*** Changes induced by *t*BuOOH (100 µM) in canalicular vacuolar accumulation (CVa) of the Bsep substrate CGamF (left panel) and the Mrp2 substrate GS-MF (right panel), in the absence or presence of the ERK1/2 inhibitor PD098059 (PD, 5 µM and 50 µM), the JNK1/2 inhibitor SP600125 (SP, 1 µM), or the $p38^{MAPK}$ inhibitor SB203580 (SB, 1 µM). IRHCs were pretreated for 15 min with the

MAPK inhibitors, or with their respective vehicles in the control group, and then with *t*BuOOH (100 µM) for a further 15-min period. Finally, IRHCs were exposed for an additional 15-min period to CGamF or CMFDA, a metabolic precursor of GS-MF. The canalicular accumulation was expressed as the percentage of the total number of IRHCs present in the field showing visible apical CGamF- or GSMF-associated fluorescence, referred to control values. At least 200 IRHCs were analyzed in each group (n = 6). Values are mean ± S.E.M. [a]Significantly different from the control group (DMSO) ($p < 0.05$); [b]significantly different from *t*BuOOH group ($p < 0.05$).

FIGURE 3. ***Protective effect of MAPK inhibitors on the changes in Bsep and Mrp2 localization induced by tBuOOH in IRHCs.*** Confocal images showing localization of (*A*) Bsep and (*B*) Mrp2, after exposure to *t*BuOOH (100 µM) for 15 min, in the absence or presence of the ERK1/2 inhibitor PD098059 (PD, 50 µM), the JNK1/2 inhibitor SP600125 (SP, 1 µM), or the $p38^{MAPK}$ inhibitor SB203580 (SB, 1 µM), administered 15 min before addition of *t*BuOOH; insets are the corresponding differential interface contrast (DIC) images. After these treatments, IRHCs were fixed and immunostained for Bsep or Mrp2, as described in *Materials and Methods*. Location of the transporters was evaluated by image analysis of the photographs obtained, by assessing the distribution pattern of fluorescence intensity along an axis perpendicular to the canalicular vacuole (4 µm to each side of the canalicular center), using the image analysis program Image J 1.34m software (Improvision, Coventry, NIH). Statistical analysis of the fluorescence profiles showed a significant change in *t*BuOOH-treated IRHCs ($p < 0.05$; number of canalicular vacuoles analyzed > 10, from 3 independent experiments per group), with a decrease in the

fluorescence intensity in the canalicular area, together with an increased fluorescence at a greater distance from the canalicular vacuole, which was counteracted by the MAPK inhibitors.

FIGURE 4. ***Effect of MAPK inhibitors on tBuOOH-induced blebbing and disruption of F-actin cytoskeleton in IRHCs.*** (*A*) Bleb formation and (*B*) changes in F-actin distribution after exposure to *t*BuOOH (100 µM) for 15 min, in the presence or absence of the ERK1/2 inhibitor PD098059 (PD, 50 µM), the JNK1/2 inhibitor SP600125 (SP, 1 µM), or the $p38^{MAPK}$ inhibitor SB203580 (SB, 1 µM), administered 15 min before *t*BuOOH addition. Bleb formation was assessed by phase-contrast microscopy. F-actin distribution was assessed by staining with fluorescently-labeled phalloidin, followed by confocal microscopy and further image analysis for quantification of the proportion of fluorescence intensity localized in the pericanalicular zone. The number of IRHCs analyzed per group was > 30, obtained from a minimum of 3 independent preparations. Values are mean ± S.E.M. [a]Significantly different from control group ($p < 0.05$); [b]Significantly different from *t*BuOOH-treated group ($p < 0.05$).

FIGURE 5. ***Effect of MAPK inhibitors on tBuOOH-induced alterations in biliary secretory function in PRLs.*** Sequential changes in (*A*) bile flow, (*B*) bile salt output, and (*C*) DNP-SG output, in *in situ* PRLs exposed to *t*BuOOH (75 µM) for 10 min, in the presence or absence of the ERK1/2 inhibitor PD098059 (PD, 5 µM), the JNK1/2 inhibitor SP600125 (SP, 1 µM), or the p38MAPK inhibitor SB203580 (SB, 250 nM), administered

15 min before *t*BuOOH. Data are expressed as mean ± S.E.M. [a]Significantly different from control; [b]Significantly different from *t*BuOOH ($p < 0.05$, $n = 5$).

FIGURE 6. ***Prevention by MAPK inhibitors of Bsep/Mrp2 endocytic internalization and F-actin cytoskeleton disruption induced by tBuOOH in PRL experiments.*** Representative confocal images illustrating the endocytic internalization of Bsep and Mrp2, together with the disruption of F-actin cytoskeleton induced by *t*BuOOH (75 µM, 10 min), and its prevention by the ERK1/2 inhibitor PD098059 (PD, 5 µM), the JNK1/2 inhibitor SP600125 (SP, 1 µM), or the $p38^{MAPK}$ inhibitor SB203580 (SB, 250 nM), administered 15 min before *t*BuOOH (or DMSO in controls). Images were taken 20 min after the onset of perfusion with *t*BuOOH. (*A*) Co-staining of Bsep (green) and F-actin (red); (*B*) Co-staining of Mrp2 (green) and F-actin (red). In control livers, both Bsep and Mrp2 were mainly confined to the canalicular space, whereas in livers treated with *t*BuOOH, relocalization of intracellular fluorescence associated with both Bsep and Mrp2 from the canalicular space to the pericanalicular area was apparent, thus indicating endocytic internalization of the transporters. The MAPK inhibitors prevented this phenomenon, as illustrated by a control-like pattern of the Bsep and Mrp2 distribution in livers preperfused with the MAPK inhibitors. Regarding cytoskeleton integrity, pericanalicular localization of F-actin was evident in control livers, while a severe disarrangement of F-actin was observed in livers perfused with *t*BuOOH. MAPK inhibitors partially prevented *t*BuOOH-induced disturbances on F-actin cytoskeleton, thus explaining their protective effects on canalicular transporter localization and function.

Figure 1

Click here to download Figure Fig1.tif

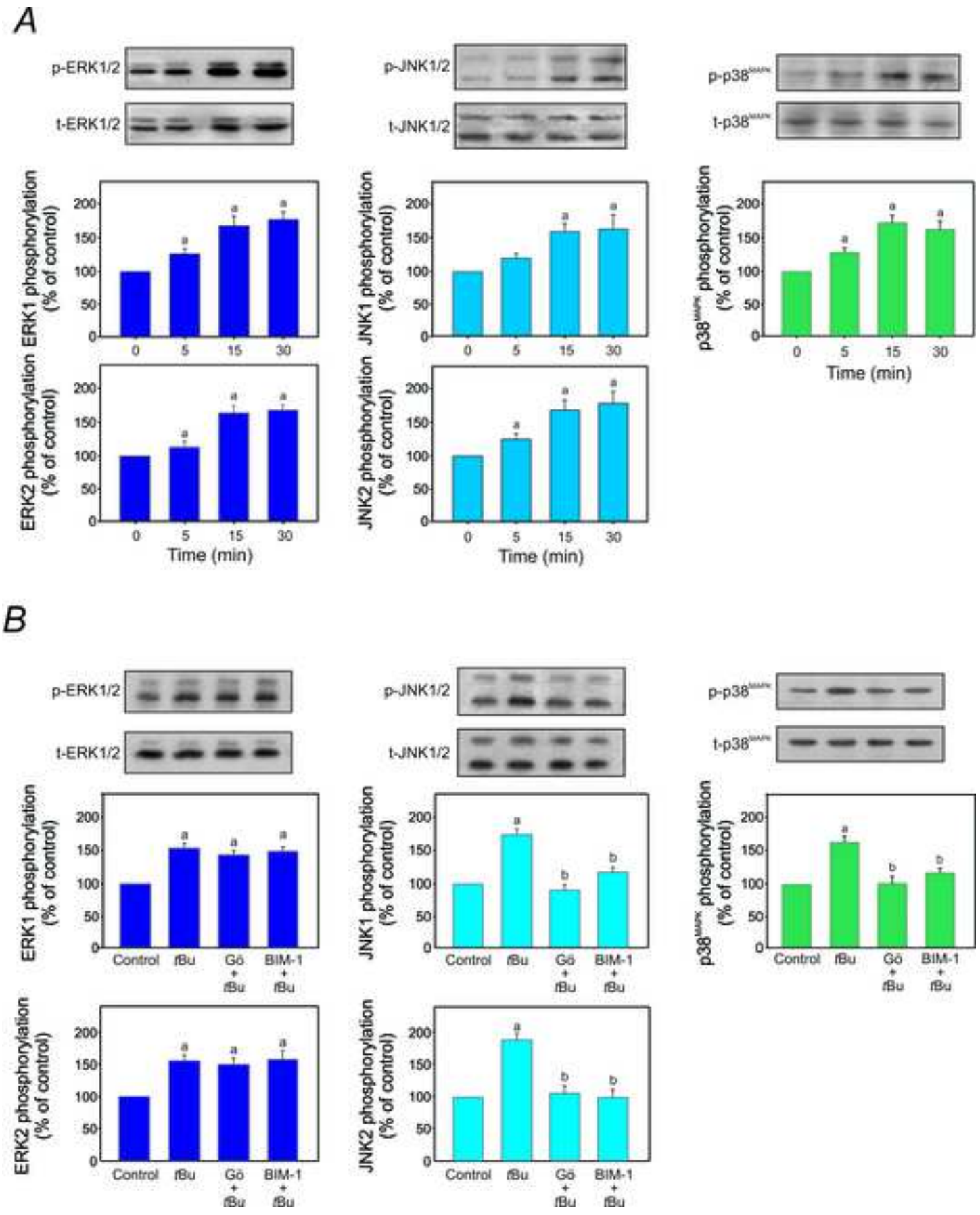

Figure 2

Click here to download Figure Fig2.tif

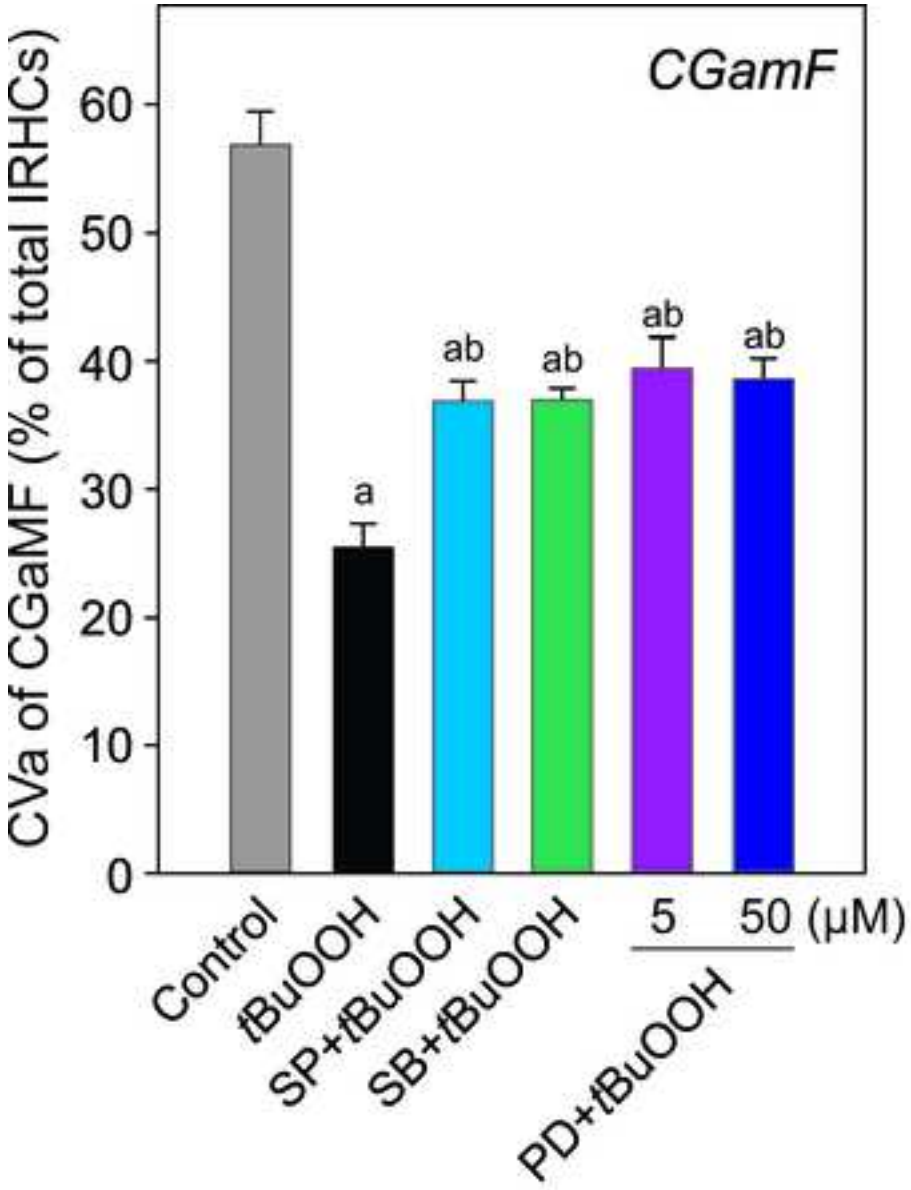

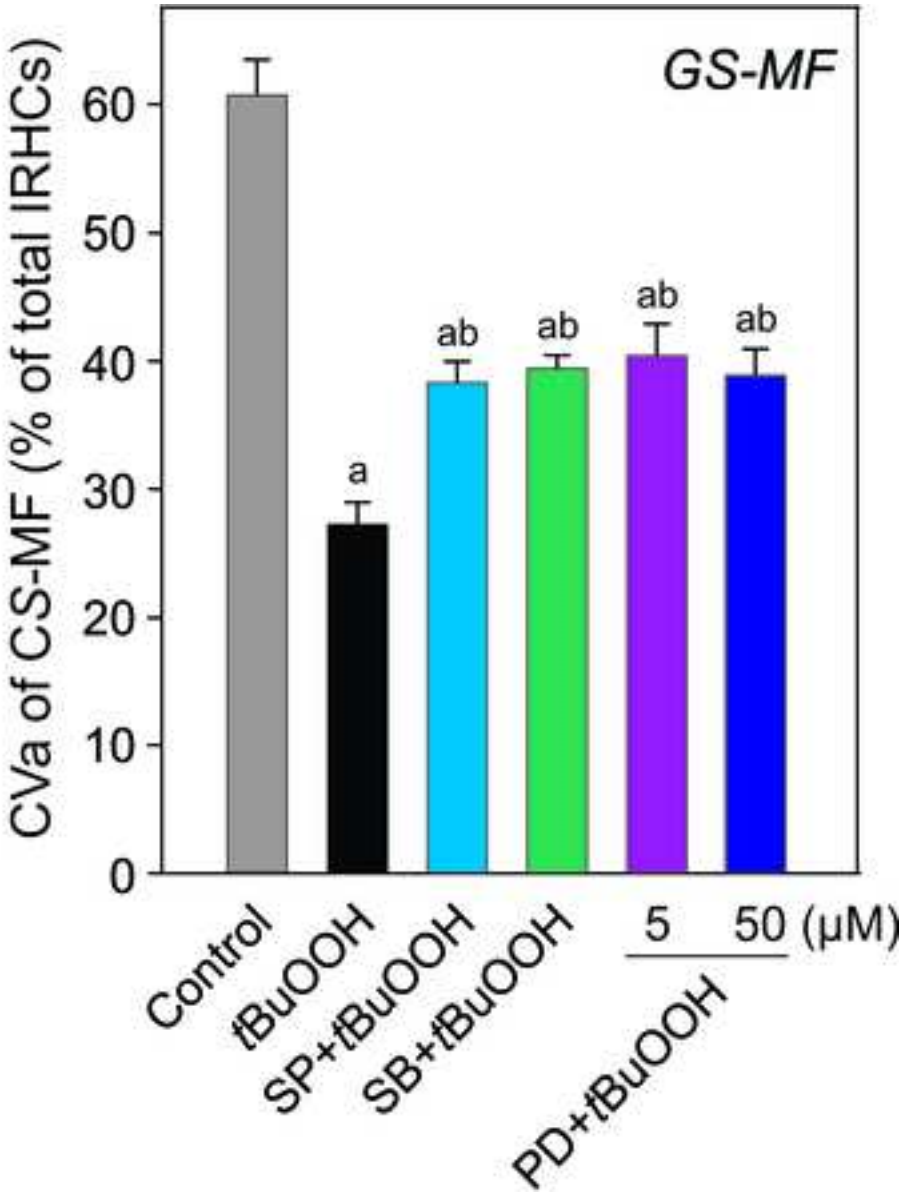

Figure 3

Click here to download Figure Fig3.tif

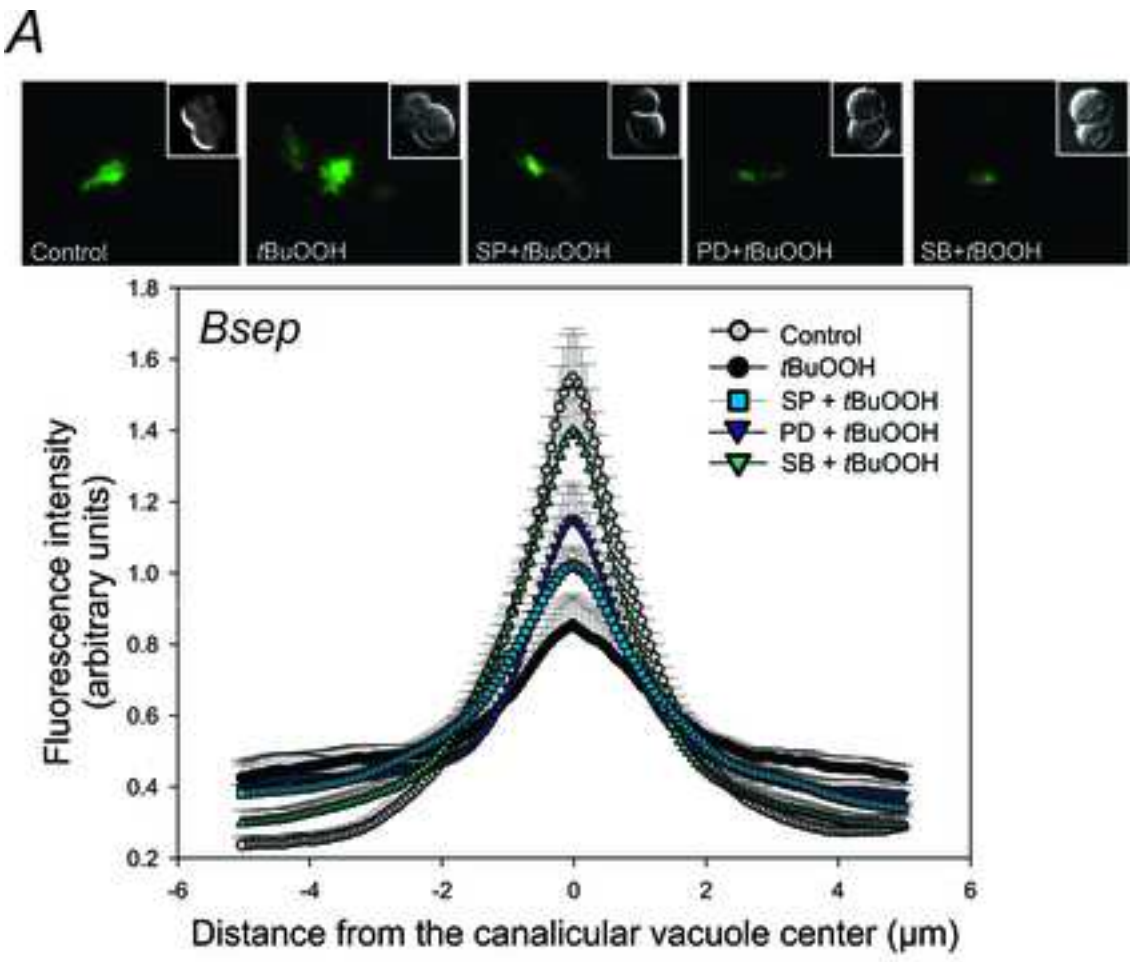

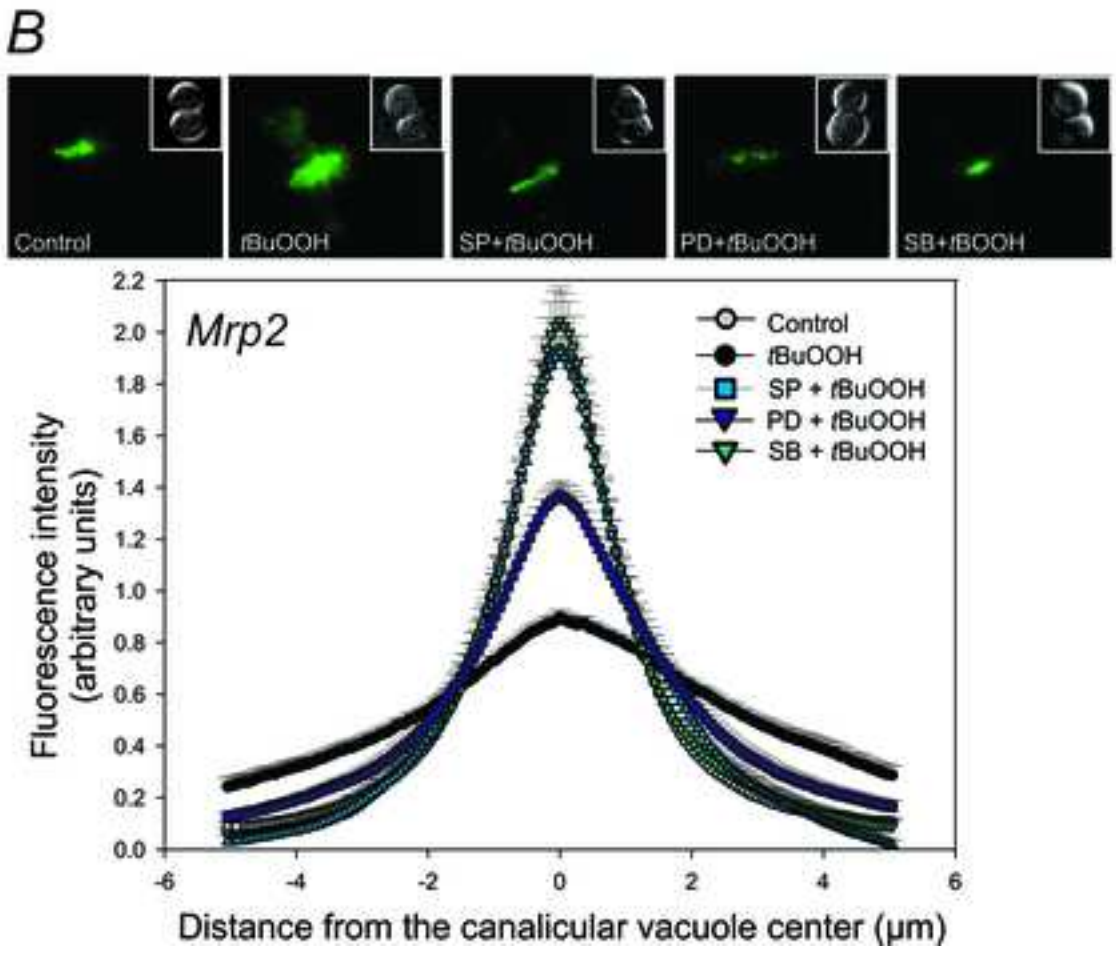

Figure 4

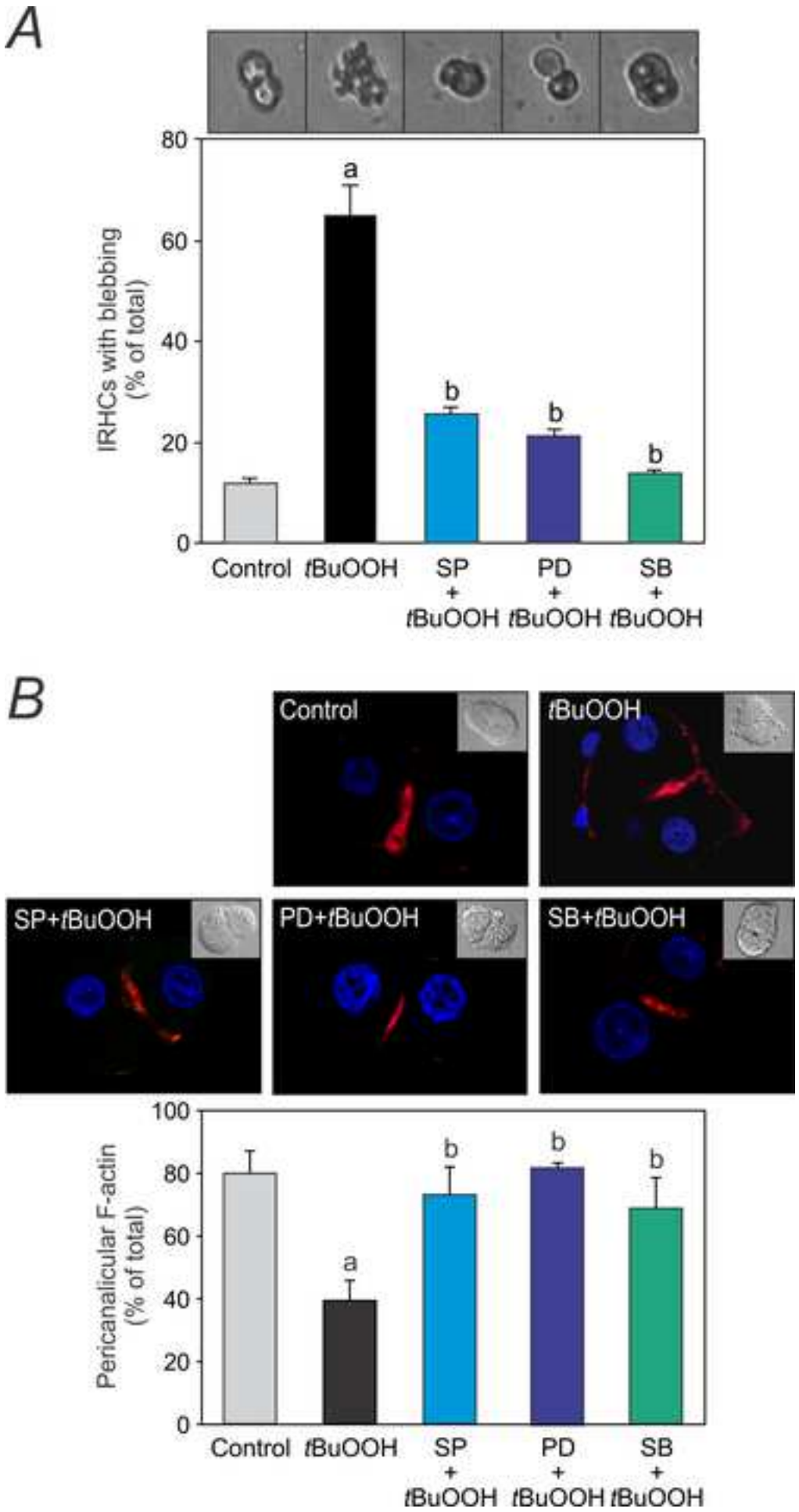

Figure 5

Click here to download Figure Fig5.tif

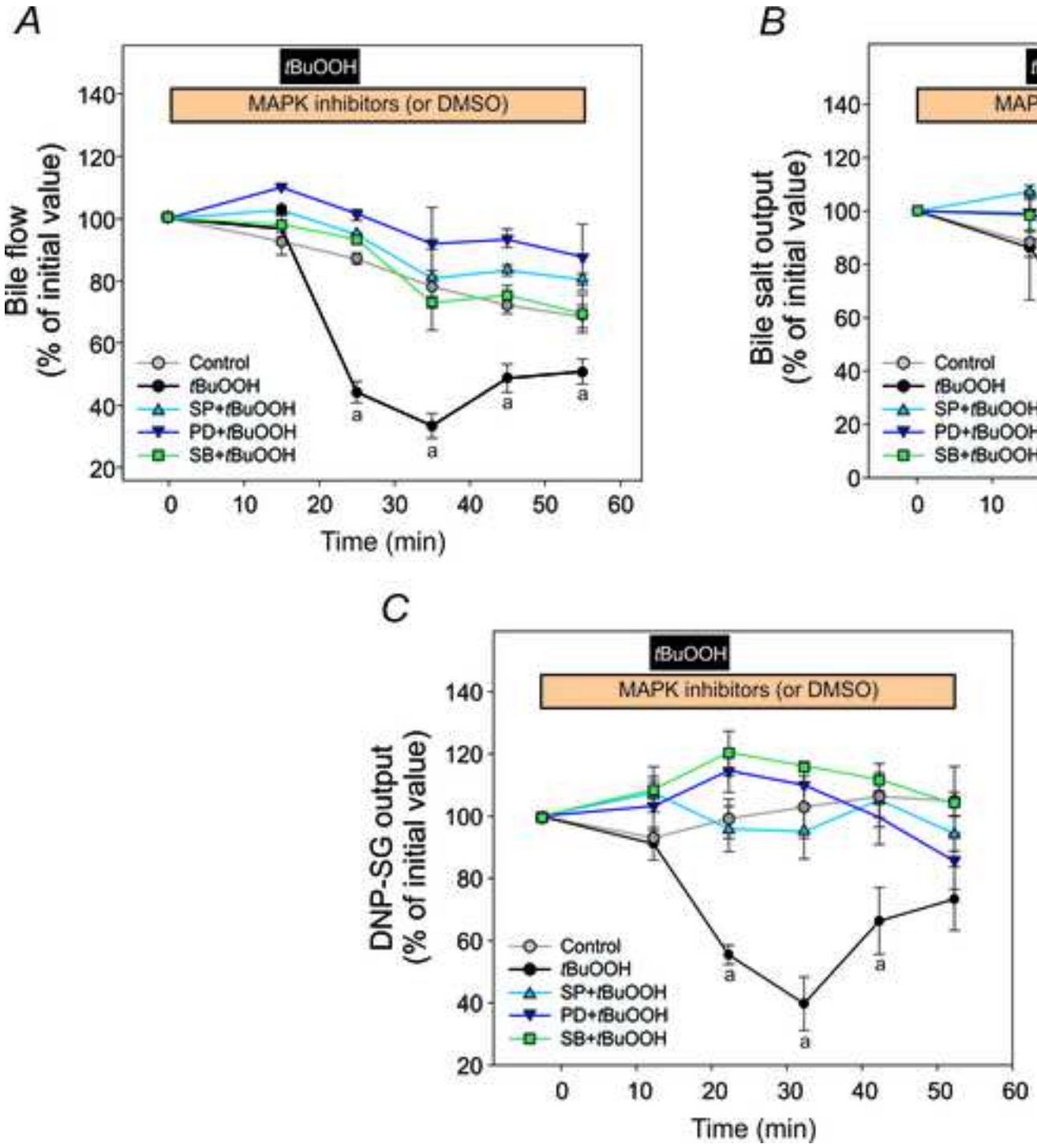

Figure 6

Click here to download Figure Fig6.tif